Received: 23 September 2022 | Accepted: 21 November 2022

DOI: 10.1002/dro2.41

RESEARCH ARTICLE

Droplet WILEY

Slippery quartz surfaces for anti-fouling optical windows

Minjing Li[1] | Tongzhen Yang[1] | Qing Yang[1] | Shaokun Wang[2] | Zheng Fang[1] | Yang Cheng[1] | Xun Hou[2] | Feng Chen[2]

[1]School of Mechanical Engineering, Xi'an Jiaotong University, Xi'an, China

[2]State Key Laboratory for Manufacturing System Engineering and Shaanxi Key Laboratory of Photonics Technology for Information, School of Electronic Science and Engineering, Xi'an Jiaotong University, Xi'an, China

Correspondence

Feng Chen, State Key Laboratory for Manufacturing System Engineering and Shaanxi Key Laboratory of Photonics Technology for Information, School of Electronic Science and Engineering, Xi'an Jiaotong University, Xi'an 710049, China.
Email: chenfeng@mail.xjtu.edu.cn

Qing Yang, School of Mechanical Engineering, Xi'an Jiaotong University, Xi'an 710049, China.
Email: yangqing@mail.xjtu.edu.cn

Funding information

International Joint Research Laboratory for Micro/Nano Manufacturing and Measurement Technologies; National Science Foundation of China, Grant/Award Numbers: 12127806, 62175195, 61875158; Fundamental Research Funds for the Central Universities

Abstract

The surface of camera-based medical devices is easily smeared by blood and fog during the surgical procedure, causing visual field loss and bringing great distress to both doctors and patients. In this article, a slippery liquid-infused porous surface (SLIPS) on a quartz window surface that can repel various liquids, especially blood droplets is reported. A femtosecond laser pulse train was used to create periodic microhole structures on the silica surface. The subsequent low surface energy treatment and lubricant infusion led to the successful preparation of a slippery surface. Such blood-repellent windows exhibited high transparency, great antifogging, and antibacterial properties. In addition, the slippery ability of the as-prepared surface exhibited outstanding stability since the surface could withstand harsh treatments/environments, such as repeated pipette scratches and immersion in different pH solutions. The as-prepared millimeter-sized quartz samples with SLIPS were attached to the endoscope lens as a protective coating and could maintain high visibility after repeated immersion in blood. We believe that the coating developed in this study will provide inspiration for the design of next-generation endoscopes or other camera-guided devices that will resist fouling, keep clear vision, and reduce operation time, thus offering great potential applications in lesion diagnosis and therapy.

INTRODUCTION

Minimally invasive medical operations are widely used in various clinical departments for their tinny incision, less pain, and rapid recovery characteristics. Endoscopes have become a crucial instrument for the internal inspection of the human body, such as duodenoscopy, laparoscopy, and colonoscopy.[1–3] However, fog and blood on the optical windows of these devices can degrade the accuracy of the monitoring data, and it can also make the picture blurred for the covering of the fouling.[4–6] In addition, microbial colonization formation on the surface of the endoscope is another factor that needs to be considered for surgery safety.[7–9] Therefore, the development of strategies for fouling control of optical instruments is urgently required.

To solve the fouling problem of the medical optical instructs, the primary way is to take out the endoscope from the body and then mechanically scrub the lens surface or rinse it with flowing water.[10] Unfortunately, repeatedly mechanical wiping can damage and wear the lens, and bring misery to the patient due to the increased operation time associated with endoscope removal. Another way to clean the lens is to combine the endoscope with additional channels through which splashing or sucking the body fluid can be applied,

which undoubtedly increases the size of the device. As for bacterial formation, it is mainly caused by the environmental bacteria adhesion during storage and the favorable conditions of the lens itself suitable for bacterial propagation.[11,12] However, it is very hard to clean the lenses thoroughly for their complex and intricate structures.

In recent years, lotus leaf-inspired superhydrophobic (SHP) surfaces with hierarchical micro to nanoscale features can effectively trap pockets of air between the solid surface and liquid droplet, resulting in an ultralow adhesion of the fluid to the surface and allowing the fluid drop to roll over the tip of the rough structure with less friction.[13–17] The remarkable characteristics enable them to repel various liquids, such as water, fog, blood, and so on.[18–23] For example, Li's group fabricated a flexible SHP surface by constructing hydrophobic SiO_2 and polydimethylsiloxane (PDMS) composite particles on the PDMS surface with a complex 3D shape.[24] When porcine blood (10 μl) was dripped onto the as-prepared surface with a tilt angle of about 10°, it easily rolled off without any residue. Nokes et al. developed an SHP surface by depositing silver and calcium on a prestressed polystyrene substrate. The surface greatly reduced blood, water, urine, and saliva adhesion.[25] However, it is very hard to maintain this property during the whole endoscopic procedure as the long-time direct contact of the cells, protein, or bacteria can greatly reduce the superhydrophobicity of the surface. More importantly, ultrahigh spectrum transmittance is difficult to achieve. To overcome the limitations of the SHP surfaces, Aizenberg and his co-works first proposed a slippery liquid-infused porous surface (SLIPS) that was inspired by the capture mechanism of the *Nepenthes* pitcher.[26] Different from SHP, a SLIPS is prepared by constructing a stable lubricating layer at the surface by infusing liquid in micro/nanoporous structures to replace the air in pores.[27,28] Because of the existence of lubricant, SLIPS can prevent direct contact between the underlying substrate and various liquids that are immiscible with the oil, thus greatly reducing the adsorption of contaminants including complex fluids (e.g., drinks and ink) and biological fluids (e.g., blood).[29–31] In addition, the SLIPS also has remarkable bending/abrasion resistance, self-healing properties, and pressure stability.[32,33] The characteristics of the SLIPS prepared on transparent materials provide a potential method to address the performance concerns in endoscopes, particularly for the mass processing technologies to create SLIPS with great liquid repellency. Most of the existing machining methods are additive, and the slippery properties are highly susceptible to loss with the destruction of the surface microstructures. Recently, femtosecond laser has been proven an effective tool to prepare SLIPS on different materials, such as polytetrafluoroethylene (PTFE), polyethylene terephthalate (PET), and stainless steel.[28,34,35] However, the construction of porous structures and achieving transparent SLIPS on quartz surfaces is rarely reported.

In this article, we present an effective way to prepare SLIPS on a quartz window by femtosecond laser ablation. A periodically arranged microporous structure was first constructed on the quartz surface by laser treatment and further modified by well-developed n-decyltrichlorosilane chemistry that offers to match the property of the silicon oil. The resultant surface exhibited strong repellency to water and blood. The optical property, durability, antifogging performance, and antibacterial capability of the SLIPS were also investigated. Finally, we applied the as-prepared surface to a commercial endoscope lens and tested the operation field of the scope after constant contact with blood. After the coated lens was repeatedly dipped in and removed from the blood 100 times, the area of the visible region was close to 100% and the lens still maintained remarkable anti-blood ability after cleaning and relubricating.

RESULTS AND DISCUSSION

Silica glass is widely used in microelectronics, optical fibers, and optical windows. Compared with optical polymer materials, silica glass shows outstanding advantages, such as excellent optical properties, high-temperature resistance, and corrosion tolerance. To generate a micro-porous structure on the sample surface, a silica substrate was ablated by a femtosecond laser using a line-by-line scanning manner. Figure 1a shows the schematic illustration of the fabrication system. The laser was focused onto the sample surface through an objective lens and the sample was moved by controlling the 3D movable stage. During the scanning process, each single pulse train formed a microhole. Meanwhile, a large number of nanoparticles were further spontaneously decorated on the ablated surface. The formation of the microholes and the nanoscale structures is ascribed to the material removal and particle recasting during the interaction of the femtosecond laser on the quartz glass. When a single pulse of the laser is injected onto the sample surface, part of the laser energy is absorbed by electrons through a series of nonlinear effects, such as multiphoton ionization, avalanche ionization, Coulomb microexplosion, and shock wave effect occurring at the focal point in an ultrashort time.[36–38] Some energy is transferred from electrons to the lattice, and then forms a high temperature/pressure plasma until the thermal equilibrium between electrons and ions appears. As the plasma instantaneously expands and erupts out of the laser-ablated area, the sample surface is permanently destroyed. The material at the focal point is removed with the plasma burst and part of the nanoscale-ejected molten particles fall back on the sample surface after resolidifying. As a result, uniform microholes are formed on the quartz after femtosecond laser ablation.

Figure 1b,c shows the scanning electron microscope (SEM) images of the femtosecond laser-irradiated silica surfaces at average distance (AD) = 4.5 μm. AD refers to the average distance of adjacent laser scanning lines. On such surfaces, abundant micro/nano hierarchical structures are randomly distributed around the microholes, some of which accumulate together to form a block. High-temperature and high-pressure plasma are formed on the silica surface during the interaction between the femtosecond laser and the silica quartz. When the sample is ablated by the first pulse train, the erupted materials cool and solidify around the microporous to form abundant nanoparticles and recast layer. As the sample moves forward, the next pulse train can refocus on the untreated region,

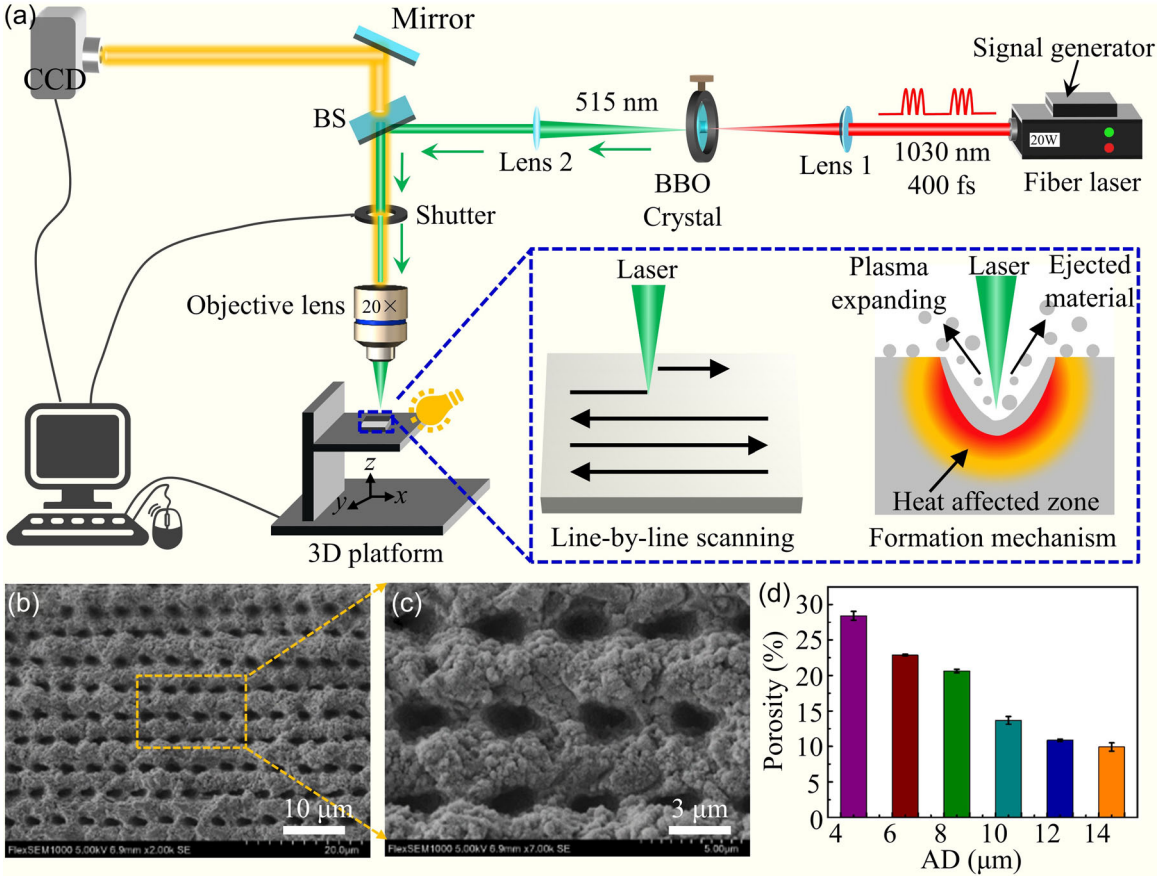

FIGURE 1 Laser fabrication system and surface topography of the porous structures. (a) Schematic illustration of the femtosecond laser micromachining system. Insets show the line-by-line scanning treatment (left) and the formation mechanism of a microhole (right). (b, c) Low- and high- magnification SEM images of the quartz surfaces after femtosecond laser ablation (AD = 4.5 μm). (d) Relationship between the porosity and the ADs.

which begins to induce a new crater and recast layer like the first hole formation. Repeating this process, periodic microhole structures are created. In addition, the formation process in the vertical direction is similar to that in the horizontal direction. When there are enough laser scan lines, a multi-hollow array structure is formed on the quartz substrate. Porosity is a very important parameter for porous structured surfaces. Figure 1d shows the dependence of the porosity on the ADs. It can be easily noticed that the porosity gradually decreases with the AD value increasing. As the AD increases, the distance between two adjacent microholes as well as the area of the laser untreated area increases, which leads to a decrease in porosity.

The fabrication process of SLIPS on silica glass surface mainly consists three steps: construction of porous structure by laser processing, low surface energy treatment, and lubricant infusion. Droplets cannot slide down on flat, rough (AD = 4.5 μm), and even chlorosilane-modified rough quartz surfaces (defined as C + Rough quartz). As shown in Figure 2a, a flat quartz surface exhibits excellent hydrophilicity with a water contact angle (CA) of 33.4°. After constructing porous structures by femtosecond laser ablation, water droplets can quickly wet the surface with a CA of nearly 0° (Figure 2b). The rapid decrease in CA is due to the laser-induced porous rough structures that amplify the intrinsic hydrophilicity of quartz glass and makes it become a superhydrophilic surface according to the Wenzel model. After the porous quartz surface is further modified with n-decyltrichlorosilane, the CA of a water droplet on such a surface is as high as 150.3° (Figure 2c). Despite the value of CA increases, the water droplet still firmly adheres to the surface and does not roll away even when the substrate is tilted at 90° because of the "micro-airbag effect"[39] (Figure 2d). The blood CA of the flat and rough quartz surfaces are 46.12° (Figure 2e) and 14.56° (Figure 2f), respectively. Although the CA increases to 147° on the C + Rough quartz surface (Figure 2g), it still sticks onto the substrate (Figure 2h). As a result, the flat, rough, and C + Rough quartz surfaces exhibit strong adhesion to both water and blood. Such surfaces can be easily wetted or polluted by these droplets. Compared with the flat, rough, and C + Rough quartz surfaces, the silicon oil-infused substrate shows a strong repellency to water and blood. These liquids can easily slide away from the slippery surface with a tilt angle of 10°, as shown in Figure 2i,j. The existence of silicone oil is equivalent to a lubricating layer, which will prevent direct contact between the liquids and the sample surface. Since water and blood, respectively, are immiscible with silicon oil, they

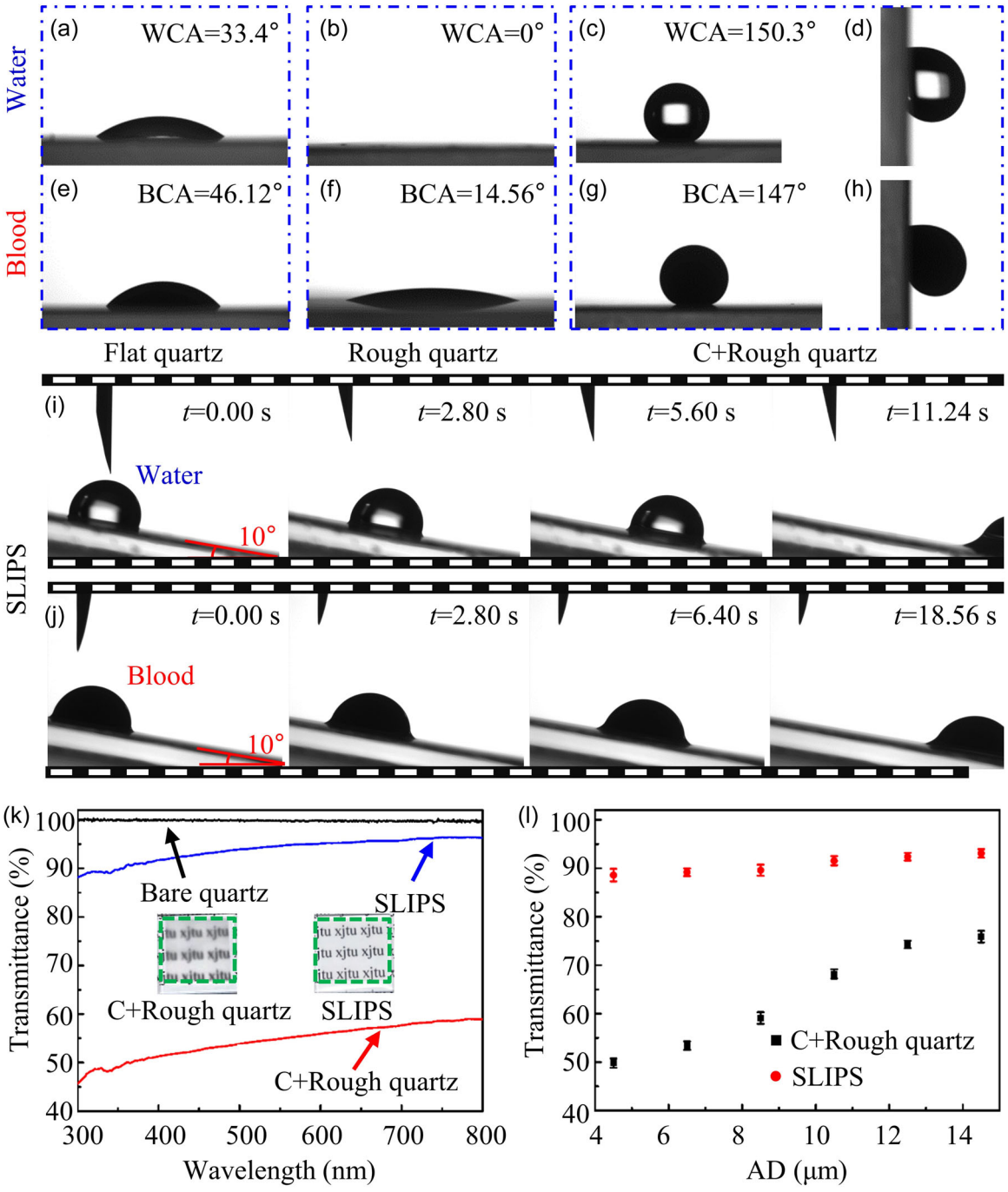

FIGURE 2 Different wettability and light transmittance of the as-prepared surfaces. Water droplet (a–d) and blood droplet (e–h) on a flat quartz surface (a, e), rough quartz surface (b, f), chlorosilane-modified rough quartz surface (c, g), and adhering onto a chlorosilane-modified rough quartz surface (d, h). (i, j) Water droplets and blood droplets sliding down the as-prepared slippery quartz surface with an incline angle of 10°, respectively. (k) Light transmittance of the bare quartz, C + rough quartz (AD = 4.5 μm), and SLIPS (AD = 4.5 μm) in the visible wavelength range. The insets are images of the entire C + rough quartz and SLIPS on a piece of paper with the letters "xjtu". (l) Variation of transmittance of the silica glass fabricated at different ADs.

float on the lubricant, which reduces the sliding resistance and enables them to slide easily away from the slippery surface. Except for the blood, the as-prepared SLIPS also exhibited strong repellence to a broad range of chemically pure or complex liquids, such as algae solution, ink, milk, and cola, as shown in Supporting Information: Figure S1 and Movies S1-4. Furthermore, the slippery performance of the as-prepared SLIPS was evaluated by the number of times that droplet (~20 μl) can slide on the tilted sample (~20°) and the results are shown in Supporting Information: Figure S2. It was found that there is a negative correlation between the sliding number and ADs.

Because the droplet takes away a small amount of lubricating oil each sliding, while the sample processed with large AD stores less lubrication, so it has fewer sliding number.

Surface roughness has a crucial influence on optical properties. Figure 2k shows the transmission spectra of the bare quartz substrate (black line), C + rough quartz (red line), and SLIPS (blue line). During the test, the transmittance of the bare quartz is considered the reference standard with a value of 100%. At the visible wavelengths, the maximum transmittance of the C + rough quartz surface is close to 60%. When the C + rough quartz substrate is placed onto a paper with black letters, it is easy to observe that the letters are blurry (left inset in Figure 2k). However, after the sample infused with silicon oil, the letters "xjtu" become very clear (right inset in Figure 2k). The remarkable visuality of the letters means the high transparency of the SLIPS and its transmittance is more than 86% in the visible spectra, which is comparable to that of bare quartz. Figure 2l shows the relationship between the transmittance and ADs. It is obvious that the transmittance of the SLIPS is consistently larger than the C + rough quartz at every processing parameter and the smaller AD, the more significant difference. As the AD increases, the surface roughness gradually decreases, and then a trend of progressive increase in light transmittance can be found. The transmittance of the laser-ablated surfaces fabricated at AD above 4.5 μm is over 85% after filling with lubricant. The good transparency is mainly attributed to the presence of lubricants.

The size of porous structures is much larger than the wavelength, which has a strong scattering effect on the incident light and leads to a poor transmittance of the C + rough quartz. When silicon oil is impregnated into the porous structure, the surface becomes flat and the refractive index contrast at the interface is reduced, thus reducing light scattering and reflection at the interface between the quartz and silicon oil.[40] The reflectance at the interface of two different media can be described by the following equation[29]:

$$R_{ab} = \left(\frac{n_a - n_b}{n_a + n_b}\right)^2, \quad (1)$$

where R_{ab} is the reflectance at the interface between material a and b, and n_a and n_b are the refractive index of a and b, respectively. It is easily obtained that a smaller reflectance occurs once these materials have closer refractive indices. Given $n_{air} = 1$, $n_{quartz} = 1.455$, $n_{siliconoil} = 1.406$, R_{aq} and R_{sq} can be calculated as 3.4% and 0.03%, respectively. The infused silicon oil greatly reduces the reflectance and scattering of the SLIPS, thus increasing the transmittance.

Fog is an important factor that leads to a blurred field of vision in endoscope surgery, so excellent anti-fogging performance is a crucial property for the as-prepared surface. To investigate this character, a bare quartz glass was used for comparison and a piece of paper with the letters "xjtu" was adhered to the backside of both samples to intuitively estimate their fog adhesion behavior. As shown in Figure 3a, the samples with a tilt angle of 45° were placed 3 cm above hot water (~90°C) and a hotplate was used to keep the continuous output of water vapor. After exposing about 120 s, the steam quickly condensed on the bare quartz surface, resulting in an opaque surface (see Figure 3b). On the contrary, the SLIPS exhibited a long-lasting antifogging performance and transparency, as shown in Figure 3c. According to the previous reports, there are two perspectives that can explain this phenomenon.[41] First, the SLIPS has a stable lubrication layer with extremely low surface energy, leading to a lower nucleation density compared with the bare quartz surface. Therefore, water droplets are less likely to nucleate on the SLIPS. Second, water droplets exhibit lower adhesive force and higher mobility on the SLIPS, which makes them more likely to coalesce with each other, as presented in sequential photographic images in Figure 3d. This combination causes the droplets to become bigger and then slide down under gravity so that the whole surface can keep good transparency.

Residual bacteria on medical devices can bring a potential threat to patient health, but this risk can be diminished by reducing bacterial adhesion.[42] The antibacterial activity was evaluated by testing the antibacterial rate of SLIPS against both Gram-positive bacteria, *Staphylococcus aureus*, and Gram-negative bacteria, *Escherichia coli* which are the most common bacteria that cause infections in the medical field. The bare quartz groups of *S. aureus* and *E. coli* were used as a positive control. As illustrated in Figure 3e, there are lots of bacteria colonies covered on the plate of the control sample. In the contrast, only a small number of colonies can be observed on the growth media of SLIPS, both toward *S. aureus* and *E. coli*, suggesting that SLIPS has good bacteria inhibition. Based on the number of colonies on the nutrient media, the number of colonies adhering to the samples was estimated, as shown in Figure 3f. In comparison with the untreated quartz, the antibacterial rate of the as-prepared SLIPS to *S. aureus* and *E. coli* is 75.7% and 76.3% (Figure 3g). The results reveal that the growth of more than 75% of bacteria can be inhibited on the quartz surface after the construction of SLIPS. Thus, the as-fabricated SLIPS has a good antibacterial ability.

The characteristics of ultrahigh transparency, antifogging performance, excellent blood adhesion resistance, and antibacterial performance endow the as-prepared SLIPS with potential application in biomedical instruments. As a proof-of-concept, a circular SLIPS sheet with a diameter of 5.5 mm was coated onto a commercial endoscope lens connected by a PDMS adhesion layer, as shown in Figure 3h. To evaluate the duration of the endoscope in such a complex environment in vivo, the novel endoscope was repeatedly immersed into and taken out from the sheep blood and characterized the loss of visibility due to the lens occlusion (Figure 3i). A print pattern with a black and white grid was used as a reference for observation. The view of the uncoated lens was immediately blocked after first contact with the blood (Figure 3j and the red line in Figure 3l). In contrast, the SLIPS-coated scope could still maintain nearly 100% visual field clarity for up to 100 dips in the blood (Figure 3k). To verify the accuracy of the results, three different samples were tested and the relationship between the percentage of the visible area and the number of dips in blood is shown in Figure 3l (purple, green, and blue lines in Figure 3l represent independent experiments performed with the samples mentioned above). It can be seen that the coated scopes keep stable

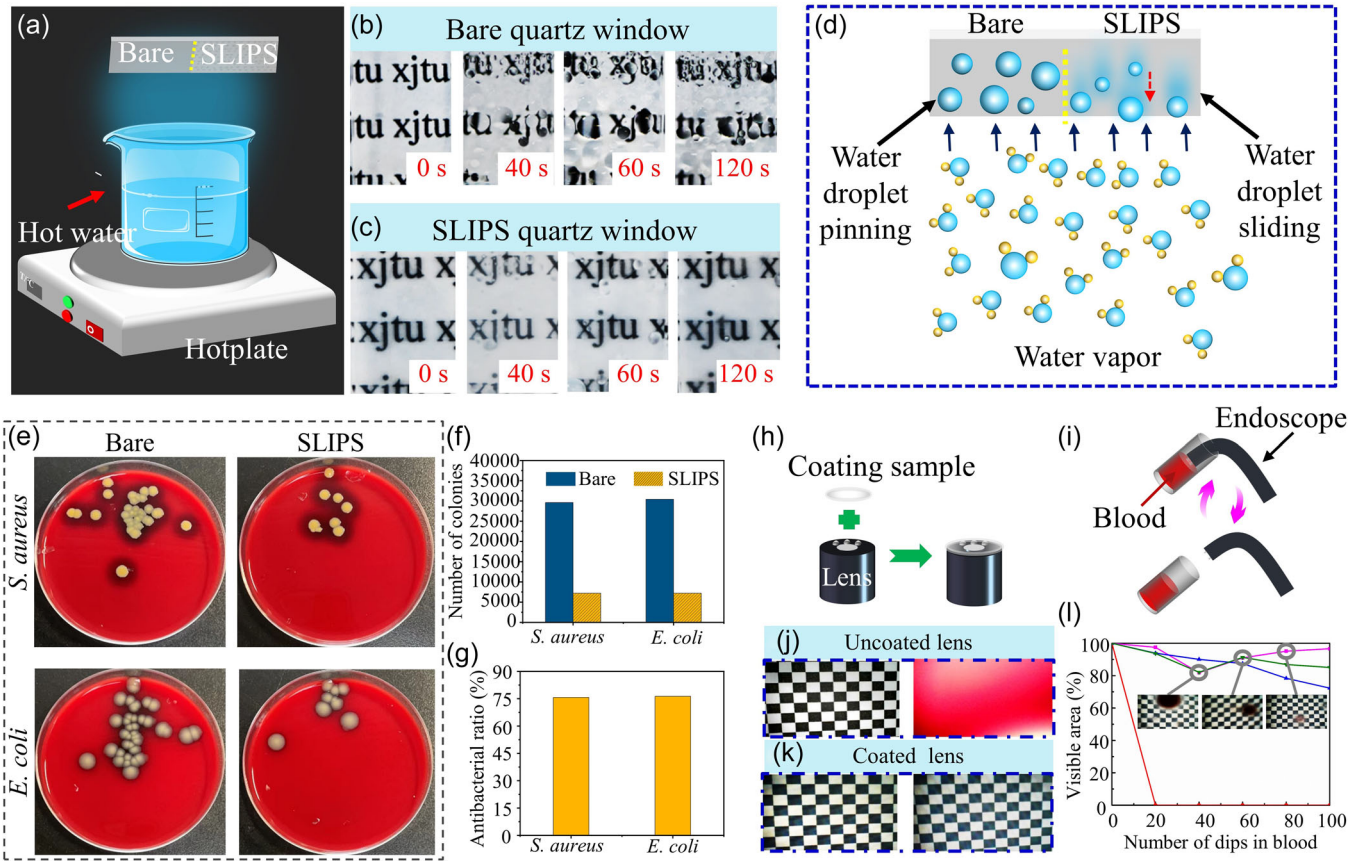

FIGURE 3 Antifogging, antibacterial performance, and concept application of the bare quartz and the slippery liquid-infused porous surface (SLIPS). (a) Schematic diagram of the setup for antifogging test. (b, c) Photographs of the bare quartz (b) and SLIPSs (c) after being held at 3 cm over the steaming water for 120 s. (d) Schematic illustration of the anti-fog mechanism for the samples. (e) Photographs of bacterial colonies of *Staphylococcus aureus* and *Escherichia coli* after incubation with bare quartz and SLIPS at 37°C for 48 h. (f) The number of *S. aureus* and *E. coli* colonies on the bare quartz and SLIPS. (g) Antibacterial rate of *S. aureus* and *E. coli*. The bare quartz was taken as a positive control. (h) Schematic illustration of the coating process: the slippery surface (diameter, 5.5 mm) adhered to the tip of the endoscope lens via a drop of polydimethylsiloxane (PDMS), and the PDMS was solidified ensuring the SLIPS tightly adhere to the surface of the lens. (i) Schematic diagram of blood dipping test. (j) Field of vision after dipping in blood for the uncoated lens. (k) Field of vision after dipping in blood for the coated lens. (l) Evolution of visible area after the blood dipping test for the uncoated/coated endoscopes. The red line refers to the conventional scope. The purple, green, and blue lines refer to three individual experiments performed with different coated scopes. Insets show digital images of the field of view at 40, 60, and 80 dips for one sample (purple line).

performance and remarkable vision clarity (purple and green lines). Even for the poorest sample (blue line), the visibility decreases by only about 25% after 100 dips because a small amount of micro-droplet attaches to the surface. However, the adhesion of the fouling is dynamic and temporary: millimeter-sized droplets are attached to the lens surface but they are not pinned. Such droplets randomly appear in the different positions of the lens surface (insets in Figure 3l). After repeated dipping, the droplets move away, the scope still has a clear field of view and the image target can be identified. More importantly, the lens that has been used for a long time can still maintain good visibility after cleaning and re-lubricating for another 100 dips (Supporting Information: Figure S3).

The mechanical and durable stability of the SLIPS were investigated. Considering the possible utilization of the as-prepared anti-fouling windows in endoscopy, the surface of the quartz may be scratched by some artificial organs, such as the endoscope passing through the plastic flaps of the patient's intubation tube. To simulate this potential mechanical damage, a pipette tip was used to randomly scratch the entire SLIPS at least 20 times, and the sliding test of a blood droplet was subsequently performed, as shown in Figure 4a. Clearly, even though the as-prepared SLIPS is damaged by the pipette many times, it still exhibits excellent blood repellence since the droplet slides down the damaged SLIPS easily (Supporting Information: Movie S5). The 3D micropores are very important to the SLIPS surface. Once the surface is mechanically damaged, the lubricant stored in the porous structures will spontaneously flow to the damaged area and reinfuse it, thereby self-repairing the damaged SLIPS. Moreover, the resistance against mechanical damage of SLIPS was further demonstrated by sandpaper abrasion, as shown in Figure 4b. It is obvious that the sliding speed decreases with extending the abrasive cycle while the sliding angle increases. However, the surface can still maintain slippery property after the

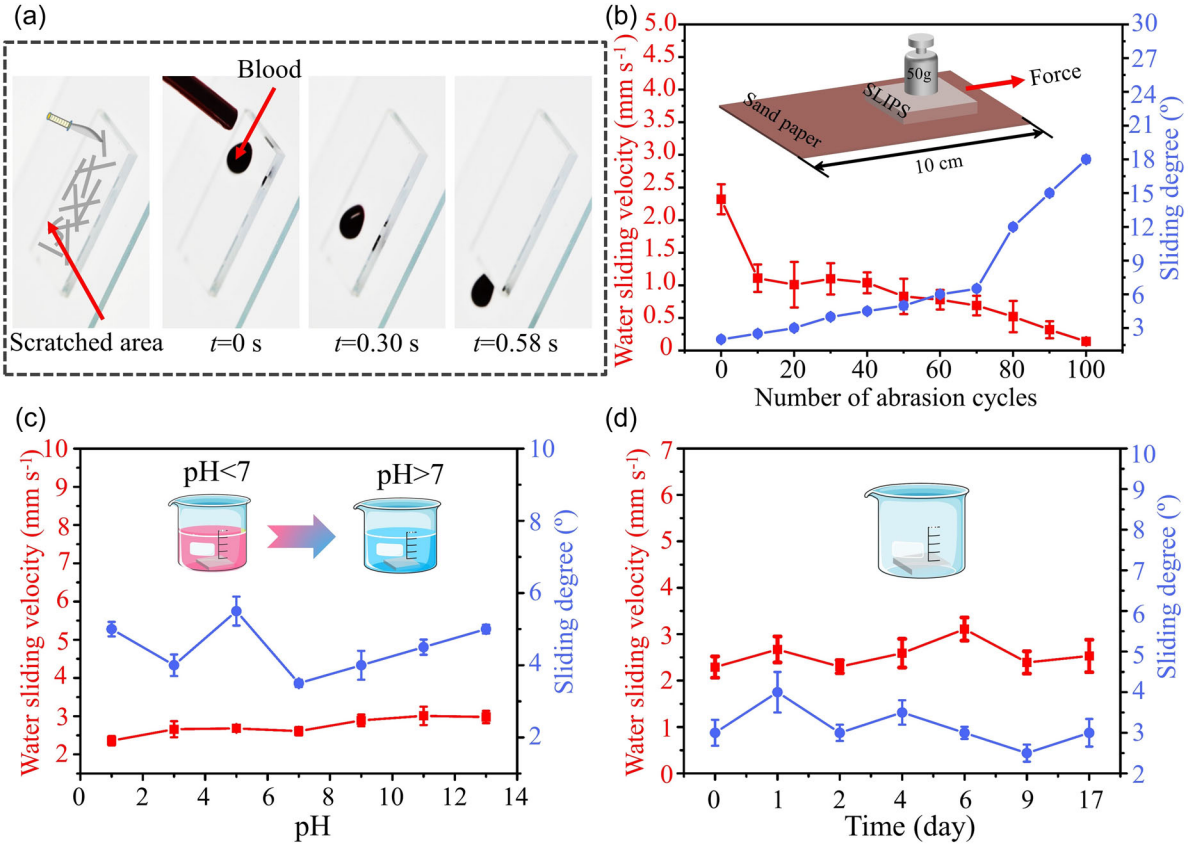

FIGURE 4 Investigation of the stability of the as-prepared slippery liquid-infused porous surface (SLIPS). (a) Sliding performance of blood droplet on the SLIPS after multiple scratches and damages. (b) Water sliding velocity and sliding angles of the SLIPS after continuous sandpaper abrasion. (c) Water sliding velocity and sliding angles of the SLIPS after immersing in different pH solutions for 30 min. (d) Water droplet sliding velocity and sliding angles with respect to time were determined by a long-term stability test.

sandpaper abrasion for 80 cycles. Since different body fluids have different pH values, such as 6.7–7.0 for extracellular fluid, 0.9–1.5 for gastric fluid, and 8.4 for intestinal fluid, it is significant to investigate the durability of the as-prepared SLIPS under different pH conditions. We measured the sliding velocities and angles of the water (7 µl) on the SLIPS that were immersed into corrosive solutions with various pH for 30 min (pH adjusted using HCl and NaOH), as shown in Figure 4c. It is obvious that the as-prepared SLIPS still maintains water repellence with a sliding angle of less than 10°. In addition, storage in air was conducted to further assess the durability of the SLIPS. As shown in Figure 4d, the slippery property exhibits no obvious change after storage in a laboratory environment for 17 days, indicating that the prepared samples have good durability.

CONCLUSION

In this article, a blood-repellent optical window was prepared on a silica glass surface by infusing lubricant into its porous microstructure fabricated by femtosecond laser ablation. The surfaces integrate the most attractive properties of previously reported SLIPS coatings, such as highly effective liquid repellency to various liquids especially for blood, great repellency after strong mechanical damage, and immersion into corrosive solutions with different pH solutions, presenting good antifogging properties. More importantly, the as-prepared SLIPS substrates have extreme transparency with transmittance in the visible spectra exceeding 86%. In addition, it can decrease the adhesion of bacteria and the antibacterial rates can reach 75.7% for *S. aureus* and 76.3% for *E. coli*. Furthermore, the slippery window can be utilized as a coating with antiwetting properties on an endoscope lens as a proof-of-concept. The coated endoscope keeps nearly 100% visual field clarity after repeatedly being immersed into and taken out from the sheep blood up to 100 dips. The presence of the coating can contribute to achieve uninterrupted inspection during the endoscopic surgery and the design of a flexible instrument without cleaning channels, offering enormous potential for disease diagnosis and treatment.

METHODS

Femtosecond laser ablation: A quartz substrate was mounted on a 3D movable platform controlled by a computer program and placed vertically in the direction of the laser incidence. Femtosecond laser

pulses with a pulse duration of 300 fs, central wavelength of 1030 nm, and repetition of 300 kHz were generated from an fs fiber laser (FemtoYL-20, YSL Photonics Co. Ltd). Through adjusting the external signal generator, the frequency of the output train was 1 kHz and each train consisted of 60 pulses. The infrared laser beam was focused onto a frequency-doubling crystal through a lens L1 to obtain a laser with a wavelength of 515 nm and collimated by lens L2. A dichroic mirror was used to split the 515 and 1030 nm laser and the 1030 nm laser was blocked. The laser power was controlled by a density filter and the shutter was utilized to control the on/off of the laser. Then, the 515 laser beam was focused onto the quartz surface using an objective lens (20×, NA = 0.40, Nikon) and used to process the sample via a line-by-line scanning method. Samples were ablated at a constant power of 0.400 W with different ADs. The AD is determined by the interval of adjacent laser scanning parameters and the scanning speed and it can be controlled by a computer program. The details of the definition can be seen in our previous work.[37] After laser ablation, the as-prepared samples were cleaned with alcohol and distilled water, respectively.

Infusion of lubricating liquid: After laser ablation, the sample was functionalized by vapor-phase deposition of fluorine-free n-decyltrichlorosilane for 2 h at room temperature to lower its surface energy. After this step, the lubricating fluid was infused into the porous structures to form a liquid lubricating layer. In this experiment, silicon oil (Aladdin, 100 mPa·s) was chosen as lubricating oil for its remarkable characteristics, such as low surface tension, less volatility, and nontoxicity. The infusion of silicon oil into the porous layer caused blood and other liquids to slide off from the SLIPS surface.

Antibacterial test: Appropriately activated Gram-positive *S. aureus* (*S. aureus*, ATCC 29213) and Gram-negative *E. coli* (*E. coli*, ATCC 25922) colonies selected from blood agar plates were put into biochemical culture solution and turbidity was adjusted to 0.5 MCF using a nephelometry. The corresponding concentration was 10^6 CFU/ml for *S. aureus* and 5×10^5 CFU/ml for *E. coli*, respectively. The bare quartz and SLIPS samples were placed in Petri dishes and 800 µl bacterial solution was added in while ensuring that the samples were completely submerged. The samples were taken out and we removed the bacterial liquid from the sample surface and they remained at room temperature for 1 h. Then, 8 ml sterile physiological saline was dripped into the samples and the samples were agitated for 1 min to wash off the bacteria attached to the material. After that, 10 µl of the washing solution was extracted with a sterile inoculation loop and was inoculated on a blood agar plate for 48 h at 37°C. Finally, the bacterial colonies were photographed and the antibacterial activities were estimated by the standard plate count method. A sample of bare quartz was a positive control. The antibacterial rate was calculated using the following equation:

$$\text{Antibaterial ratio} = \frac{N_p - N_s}{N_p} \times 100\%. \quad (2)$$

N_p and N_s are the number of bacterial colonies on the bare quartz and SLIPS, respectively.

Endoscope experiment: The as-prepared SLIPS quartz sheet with a diameter of 5.5 mm was attached to a rigid commercial endoscope lens (Y16, OEM) by using a PDMS adhesion layer. Specifically speaking, the PDMS prepolymer and curing agent were mixed at a 10:1 ratio using the Sylgard™ 184 Silicone Elastomer and eliminated bubbles via a vacuum drying chamber. Then, a drop of liquid PDMS was dripped onto the tip of the scope and the SLIPS was gently placed on the top. The PDMS was cured in a high-temperature environment provided by a heating resistance rod. Finally, the endoscope lens and a smartphone (Mi10 Ultra, Xiaomi) were connected via a USB cable. For the dipping test, the endoscopes were repeatedly immersed into or withdrawn from the blood and characterized the visible area percentage of the lens.

Characterization: The surface morphology was measured through scanning electron microscopy (FlexSEM1000, HITACHI). The wettabilities of a water droplet (4 µl) and blood droplet (4 µl) on different quartz surfaces were investigated using a CA system (JC2000D, Powereach). The blood was sterile defibrinated sheep blood (Huayueyang Biotech. Co., Ltd.). The transmittance spectra in the wavelength range of 300–800 nm were measured using a UV-visible near-infrared spectrophotometer (PE, Lambda950). The transmittance of the samples fabricated at different ADs was obtained by testing the light power before and after passing through a quartz substrate. A He-Ne laser (wavelength = 632 nm, output power = 0.96 mW).

ACKNOWLEDGMENTS

This work is supported by the National Science Foundation of China under the Grant nos. 12127806 , 62175195 , 61875158, the International Joint Research Laboratory for Micro/Nano Manufacturing and Measurement Technologies, the Fundamental Research Funds for the Central Universities.

CONFLICT OF INTEREST

The authors declare no conflict of interest.

ORCID

Feng Chen http://orcid.org/0000-0002-7031-7404

REFERENCES

1. Harrel SK, Wilson Jr TG, Rivera-Hidalgo F. A videoscope for use in minimally invasive periodontal surgery. *J Clin Periodontol*. 2013;40:868-874.
2. Li J, Thiele S, Quirk BC, et al. Ultrathin monolithic 3D printed optical coherence tomography endoscopy for preclinical and clinical use. *Light Sci Appl*. 2020;9:124.
3. Peters BS, Armijo PR, Krause C, Choudhury SA, Oleynikov D. Review of emerging surgical robotic technology. *Surg Endosc*. 2018;32:1636-1655.
4. Lawrentschuk N, Fleshner NE, Bolton DM. Laparoscopic lens fogging: a review of etiology and methods to maintain a clear visual field. *J Endourol*. 2010;24:905-913.
5. Kalra G, Keir J, Tahery J. Prevention of blood staining of endoscope tip during functional endoscopic sinus surgery: sleeve technique. *J Laryngol Otol*. 2009;123:1358-1359.

6. Kreeft D, Arkenbout EA, Henselmans PWJ, van Furth WR, Breedveld P. Review of techniques to achieve optical surface cleanliness and their potential application to surgical endoscopes. *Surg Innov*. 2017;24:509-527.
7. Balan GG, Sfarti CV, Chiriac SA, Stanciu C, Trifan A. Duodenoscope-associated infections: a review. *Eur J Clin Microbiol Infect Dis*. 2019;38:2205-2213.
8. Ciccozzi M, Cella E, Lai A, et al. Phylogenetic analysis of multi-drug resistant *Klebsiella pneumoniae* strains from duodenoscope biofilm: microbiological surveillance and reprocessing improvements for infection prevention. *Front Public Health*. 2019;7:219.
9. Bai S, Li X, Zhao Y, Ren L, Yuan X. Antifogging/antibacterial coatings constructed by N-hydroxyethylacrylamide and quaternary ammonium-containing copolymers. *ACS Appl Mater Interfaces*. 2020;12:12305-12316.
10. Sunny S, Cheng G, Daniel D, et al. Transparent antifouling material for improved operative field visibility in endoscopy. *Proc Natl Acad Sci*. 2016;113:11676-11681.
11. Johani K, Hu H, Santos L, et al. Determination of bacterial species present in biofilm contaminating the channels of clinical endoscopes. *Infect Dis Health*. 2018;23:189-196.
12. Kovaleva J. Endoscope drying and its pitfalls. *J Hosp Infect*. 2017;97:319-328.
13. Yong J, Yang Q, Hou X, Chen F. Nature-inspired superwettability achieved by femtosecond lasers. *Ultrafast Science*. 2022;2022:9895418.
14. Gong D, Long J, Jiang D, et al. Robust and stable transparent superhydrophobic polydimethylsiloxane films by duplicating via a femtosecond laser-ablated template. *ACS Appl Mater Interfaces*. 2016;8:17511-17518.
15. Movafaghi S, Leszczak V, Wang W, et al. Hemocompatibility of superhemophobic titania surfaces. *Adv Healthcare Mater*. 2017;6:1600717.
16. Sun T, Tan H, Han D, Fu Q, Jiang L. No platelet can adhere—largely improved blood compatibility on nanostructured superhydrophobic surfaces. *Small*. 2005;1:959-963.
17. Yong J, Yang Q, Chen F, et al. Stable superhydrophobic surface with hierarchical mesh-porous structure fabricated by a femtosecond laser. *Appl Phys A*. 2013;111:243-249.
18. Cao Y, Salvini A, Camaiti M. One-step fabrication of robust and durable superamphiphobic, self-cleaning surface for outdoor and in situ application on building substrates. *J Colloid Interface Sci*. 2021;591:239-252.
19. Davis A, Surdo S, Caputo G, Bayer IS, Athanassiou A. Environmentally benign production of stretchable and robust superhydrophobic silicone monoliths. *ACS Appl Mater Interfaces*. 2018;10:2907-2917.
20. Li M, Yang Q, Chen F, et al. Integration of great water repellence and imaging performance on a superhydrophobic PDMS microlens array by femtosecond laser microfabrication. *Adv Eng Mater*. 2018;21:1800994.
21. Lin Y, Han J, Cai M, et al. Durable and robust transparent superhydrophobic glass surfaces fabricated by a femtosecond laser with exceptional water repellency and thermostability. *J Mater Chem A*. 2018;6:9049-9056.
22. Liu C, Liao S-C, Song J, et al. A high-efficiency superhydrophobic plasma separator. *Lab Chip*. 2016;16:553-560.
23. Xi M, Yong J, Chen F, Yang Q, Hou X. A femtosecond laser-induced superhygrophobic surface: beyond superhydrophobicity and repelling various complex liquids. *RSC Adv*. 2019;9:6650-6657.
24. Li Z, Nguyen BL, Cheng YC, Xue J, MacLaren G, Yap CH. Durable, flexible, superhydrophobic and blood-repelling surfaces for use in medical blood pumps. *J Mater Chem B*. 2018;6:6225-6233.
25. Nokes JM, Liedert R, Kim MY, et al. Reduced blood coagulation on roll-to-roll, shrink-induced superhydrophobic plastics. *Adv Healthcare Mater*. 2016;5:593-601.
26. Wong TS, Kang SH, Tang SKY, et al. Bioinspired self-repairing slippery surfaces with pressure-stable omniphobicity. *Nature*. 2011;477:443-447.
27. Wang C, Guo Z. A comparison between superhydrophobic surfaces (SHS) and slippery liquid-infused porous surfaces (SLIPS) in application. *Nanoscale*. 2020;12:22398-22424.
28. Yong J, Chen F, Yang Q, et al. Nepenthes inspired design of self-repairing omniphobic slippery liquid infused porous surface (SLIPS) by femtosecond laser direct writing. *Adv Mater Interfaces*. 2017;4:1700552.
29. Nishioka S, Tenjimbayashi M, Manabe K, et al. Facile design of plant-oil-infused fine surface asperity for transparent blood-repelling endoscope lens. *RSC Adv*. 2016;6:47579-47587.
30. Zhang P, Chen H, Zhang L, Ran T, Zhang D. Transparent self-cleaning lubricant-infused surfaces made with large-area breath figure patterns. *Appl Surf Sci*. 2015;355:1083-1090.
31. He W, Liu P, Zhang J, Yao X. Emerging applications of bioinspired slippery surfaces in biomedical fields. *Chem A Eur J*. 2018;24:14864-14877.
32. Deng R, Shen T, Chen H, Lu J, Yang H-C, Li W. Slippery liquid-infused porous surfaces (SLIPSs): a perfect solution to both marine fouling and corrosion? *J Mater Chem A*. 2020;8:7536-7547.
33. Baumli P, Teisala H, Bauer H, et al. Flow-induced long-term stable slippery surfaces. *Adv Sci*. 2019;6:1900019.
34. Yong J, Huo J, Yang Q, et al. Femtosecond laser direct writing of porous network microstructures for fabricating super-slippery surfaces with excellent liquid repellence and anti-cell proliferation. *Adv Mater Interfaces*. 2018;5:1701479.
35. Fang Y, Yong J, Cheng Y, Yang Q, Hou X, Chen F. Liquid infused slippery stainless steel surface prepared by alcohol-assisted femtosecond laser ablation. *Adv Mater Interfaces*. 2021;8:2001334.
36. Butkutė A, Jonušauskas L. 3D manufacturing of glass microstructures using femtosecond laser. *Micromachines*. 2021;12:499.
37. Li M, Yang T, Yang Q, et al. Bioinspired anti-fogging and anti-fouling artificial compound eyes. *Adv Opt Mater*. 2022;10:2200861.
38. Chen F, Deng Z, Yang Q, et al. Rapid fabrication of a large-area close-packed quasi-periodic microlens array on BK7 glass. *Opt Lett*. 2014;39:606-609.
39. Yong J, Chen F, Yang Q, et al. Controllable adhesive superhydrophobic surfaces based on PDMS microwell arrays. *Langmuir*. 2013;29:3274-3279.
40. Tenjimbayashi M, Togasawa R, Manabe K, et al. Liquid-infused smooth coating with transparency, super-durability, and extraordinary hydrophobicity. *Adv Funct Mater*. 2016;26:6693-6702.
41. Durán IR, Laroche G. Water drop-surface interactions as the basis for the design of anti-fogging surfaces: theory, practice, and applications trends. *Adv Colloid Interface Sci*. 2019;263:68-94.
42. Neoh KG, Li M, Kang E-T, Chiong E, Tambyah PA. Surface modification strategies for combating catheter-related complications: recent advances and challenges. *J Mater Chem B*. 2017;5:2045-2067.

SUPPORTING INFORMATION

Additional supporting information can be found online in the Supporting Information section at the end of this article.

How to cite this article: Li M, Yang T, Yang Q, et al. Slippery quartz surfaces for anti-fouling optical windows. *Droplet*. 2022;e41. doi:10.1002/dro2.41